Classifying the Photophysical Dynamics of Single- and Multiple-Chromophoric Molecules by Single Molecule Spectroscopy

ARTICLE *in* THE JOURNAL OF PHYSICAL CHEMISTRY A · SEPTEMBER 1998

Impact Factor: 2.69 · DOI: 10.1021/jp981808x

5 AUTHORS, INCLUDING:

Dehong Hu
Pacific Northwest National Laboratory
89 PUBLICATIONS **4,590** CITATIONS
SEE PROFILE

David Anton Vanden Bout
University of Texas at Austin
132 PUBLICATIONS **2,974** CITATIONS
SEE PROFILE

Classifying the Photophysical Dynamics of Single- and Multiple-Chromophoric Molecules by Single Molecule Spectroscopy

Wai-Tak Yip, Dehong Hu, Ji Yu, David A. Vanden Bout, and Paul F. Barbara*

University of Minnesota, Department of Chemistry, Minneapolis, Minnesota 55455

Received: April 9, 1998; In Final Form: June 26, 1998

The single molecule fluorescence spectroscopy of various isolated single-chromophoric dye molecules and multiple-chromophoric conjugated polymer molecules has been investigated. For each system the transient fluorescence "intensity", $I_{CW}(t)$ (i.e., detected photons/dwell time), has been recorded with continuous wave (CW) irradiation. $I_{CW}(t)$ has been analyzed to yield an occurrence histogram for the different "intensities", $H(I)$, and an intensity time-autocorrelation function $C_I(t)$. The histograms $H(I)$ for the various examples show highly diverse behavior with one, two, or even three peaks as well as "flat regions". The different features in the histograms are shown to arise from distinct photophysical processes. From the study of model systems, characteristic features in the intensity histograms and autocorrelation functions are shown to result from photon shot noise, "blinking" due to triplet bottlenecks, spectral diffusion due to environmental fluctuations, and interchromophoric energy transfer. Classification of the relevant photophysical processes is aided by single molecule spectroscopic data on these systems, including wavelength-resolved emission spectroscopy and "two-color excitation spectroscopy", as well as stochastic simulations. The results indicate that a combined analysis of $H(I)$ and $C_I(t)$ is a valuable approach in sorting out single molecule behavior involving multiple photophysical processes in complex systems. For single molecule systems that exhibit "on−off blinking" involving the formation of dark states, the paper also explores the practical advantages of studying the duration histograms ($H(t_{on})$ and $H(t_{off})$) versus the intensity autocorrelation function $C_I(t)$, for quantifying the underlying photophysical dynamics.

I. Introduction

Single molecule spectroscopy[1−4] is playing an ever increasing role in the investigation of molecular dynamics of complex systems including single dye molecules in polymer films,[4−7] biomolecules with covalently attached fluorescent probes,[8−12] complex multichromophoric conjugated polymer molecules,[13] and isolated molecular assemblies such as the photosynthetic light-harvesting complexes.[14] Single molecule spectroscopy has allowed for the investigation of molecular processes that are difficult to study, if not completely obscured, by the averaging that is inherent in ensemble measurements. Some of the processes that have been investigated include spectral diffusion of molecules due to thermal and photochemically driven environmental dynamics,[6,15−17] the complex kinetics/dynamics associated with intramolecular energy transfer in bichromophoric[18] and multichromophoric molecules,[13,19] and single molecule chemical and photophysical kinetics.[20−22]

A common experimental approach in single molecule spectroscopy is to spatially resolve the fluorescence signals from highly dilute thin-film samples of immobilized single absorbing/fluorescent molecules that are widely separated (i.e., >1 μm). For single molecule spectroscopy, the molecules are typically studied one at a time by focusing the laser to a diffraction-limited spot and centering the molecule of interest at the laser focal volume. The fluorescence from the molecule is collected, and the intensity, polarization,[12] and spectrum can be studied for each particular molecule. Notch and band-pass filters are commonly used to prevent the excitation light from reaching the detector.

The total time a molecule can be studied and the total number of photons emitted are severely limited by the eventual irreversible photochemistry of the molecule known as "photobleaching". Under usual irradiation conditions (200 W cm^{-2}), fluorescent molecules are excited on the order of 10^5 s^{-1} and survive for tens to hundreds of seconds (at room temperature). It is important, therefore, to make the most of the signal that is obtained. The highest signal-to-noise single molecule fluorescence data is the wavelength-integrated emission intensity, $I_{CW}(t)$, as a function of irradiation time with continuous wave (CW) laser light. The fluorescence "intensity" is measured by single-photon-counting detection. The experimental data $I_{CW}(t)$, therefore, are of the form detected photons/dwell time.

The present paper is concerned with the investigation and analysis of the fluorescence intensity fluctuations of a variety of single-chromophoric and multiple-chromophoric single molecules, toward the goal of unraveling the underlying photophysical dynamics. For such molecules, fluctuations of $I_{CW}(t)$ have been analyzed to quantitatively characterize the underlying single molecule dynamics.[15,20] We are particularly concerned with ambient temperature measurements with only moderate laser excitation intensities for which coherent high-intensity effects such as photon antibunching can be ignored.[23]

One commonly observed source of single molecule intensity fluctuations involves discrete intensity jumps from an "on" (high) to an "off" (background) intensity level due to quantum jumps of the single molecule to long-lived nonemissive "dark" states. This effect has often been denoted by the term "blinking".[24] A common source of blinking in simple fluorescent dye molecules involves intersystem crossing to a long-lived triplet dark state, as summarized in Figure 1. Here E_{det} is the efficiency of detecting an emitted photon and k_{exc} is the molecular excitation rate, which is proportional to the laser intensity, I_{laser}, and the cross section for absorption at the laser wavelength, $\sigma(S_0 \rightarrow S_1)$. Well-known expressions for the *average duration* of the "on" and "off" states, τ_{on} and τ_{off}, respectively, are summarized in Figure 1.[25] Besides long-lived

* To whom correspondence should be addressed.

S1089-5639(98)01808-8 CCC: $15.00
Published on Web 09/09/1998

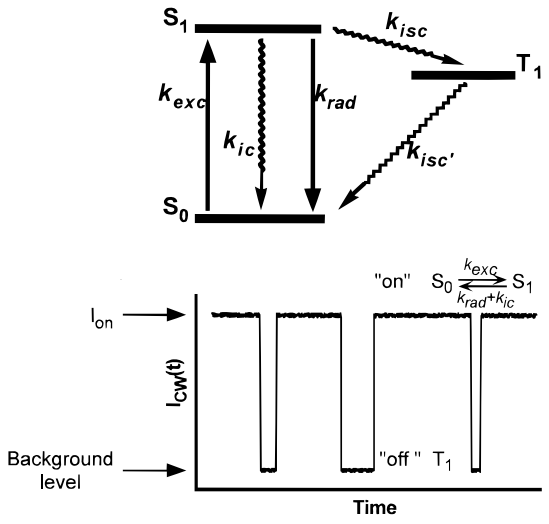

$$I_{on} = k_{exc}\frac{k_{rad}}{k_{rad}+k_{ic}+k_{isc}}E_{det}$$

$$\frac{1}{\tau_{on}} = k_{exc}\frac{k_{isc}}{k_{rad}+k_{ic}+k_{isc}}$$

$$\frac{1}{\tau_{off}} = k_{isc'}$$

Figure 1. Three-electronic-state model to account for the blinking behavior of single molecules. The lower panel shows an ideal $I_{CW}(t)$ for this model.

triplet sates, dark states have also been attributed to metastable ground-state isomers in some cases.[21]

Another well-known source of fluctuations in $I_{CW}(t)$ is thermally and/or photochemically driven fluctuations of the environment about each molecule, which in turn, affects the absorption spectrum, i.e., spectral diffusion.[15−17] As a result of spectral diffusion, the molecular absorption cross section $\sigma(S_0 \rightarrow S_1)$ at the laser excitation wavelength fluctuates. This leads to a corresponding fluctuation of k_{exc} and $I_{CW}(t)$. Alternatively, for single molecules that can rotate on the observation time scale, fluorescence intensity fluctuations can results from geometric and polarization effects on the excitation rate and efficiency of detection.[12] Finally, for complex molecules with more than one chromophore, such as multiple dye labeled biomolecules, and multichromophoric systems, such as fluorescent conjugated polymers,[13] the intensity fluctuation can involve several intensity levels and may be characterized by an exceedingly complex photophysical behavior.

In analogy to ensemble investigations of chemical kinetics and dynamics, it is of course necessary to employ an appropriate photodynamic model for the modeling and analysis of $I_{CW}(t)$ for a specific chemical system. This can be a difficult task, however, since spectral diffusion, "blinking" and other more complex effects may occur simultaneously for the same molecule under a specific set of conditions. A variety of powerful single molecule spectroscopic approaches that go beyond the simple $I_{CW}(t)$ measurement have been developed that aid in the unraveling of the photophysical process of specific single molecule systems. These techniques include time- and wavelength-resolved fluorescence spectroscopy,[15] time- and polarization-resolved spectroscopy,[12] and time-correlated single-photon-counting spectroscopy using ultrafast laser excitation.[6,26] These techniques, however, exhibit a smaller signal-to-noise ratio than the basic $I_{CW}(t)$ measurement because the data are resolved along another dimension (e.g., wavelength, polarization, etc.).

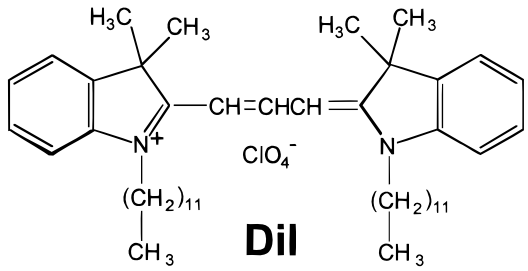

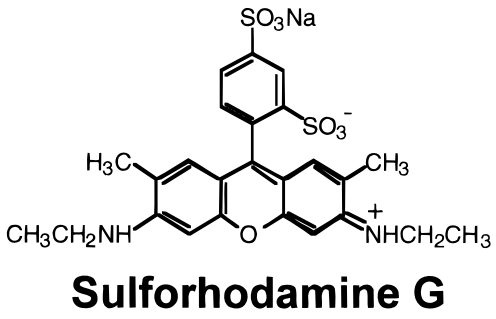

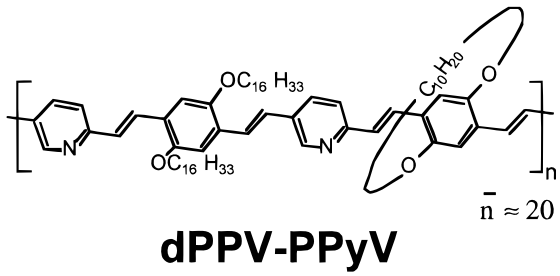

Figure 2. Molecular structures of DiI, sulforhodamine G, and the conjugated copolymer dPPV-PPyV.

The present paper explores how a detailed analysis of $I_{CW}(t)$ itself can give a surprising amount of insight into the underlying excited state dynamics and aid in the classification of relevant photophysical processes. New single molecule spectroscopic data for the relatively simple dye molecules 1,1′-didodecyl-3,3,3′,3′-tetramethylindocarbocyanine perchlorate (DiI) and sulforhodamine G and for the conjugated fluorescent polymer dPPV-PPyV (Figure 2) are presented, analyzed, and modeled. In particular, an analysis of the intensity histogram of $I_{CW}(t)$, denoted by $H(I)$, for each system reveals that the previously identified photophysical processes, including triplet bottlenecks blinking,[27] spectral diffusion,[15] and intramolecular energy transfer, give characteristic features in $H(I)$. $H(I)$ may contain one or more peaks with varying widths ranging from the Poisson shot noise limit to much broader values due to additional photophysical processes. Dependent on the underlying photophysical process that causes the additional fluctuation in $I_{CW}(t)$, the peaks in $H(I)$ can be either symmetric or asymmetric. For extremely complex molecules/assemblies that are not amenable to a simple photodynamic model, such as dPPV-PPyV, the $H(I)$ is shown to be a critical first step in characterizing the underlying photophysical processes. Furthermore, the recently introduced "two-color excitation spectroscopy" (in which the laser excitation wavelengths is rapidly switched between two colors) is shown to be a powerful and high signal-to-noise method for distinguishing between spectral diffusion and other photophysical processes that lead to fluctuations in $I_{CW}(t)$.

II. Experimental Section

DiI samples were prepared by spin casting a 1 g/L solution of poly(methyl methacrylate) (PMMA) (Aldrich) in toluene onto a glass coverslip, which was followed by adding one drop of 10^{-10} M DiI (Molecular Probe) in methanol on top of the PMMA film. Fluorescent sphere samples were prepared by spraying an appropriately diluted aqueous solution of 20 nm fluorescent latex spheres (Molecular Probe) onto a glass coverslip. dPPV-PPyV copolymer ($M_w \approx 22\,000$) was synthesized according to standard procedure.[28] dPPV-PPyV/polystyrene films were prepared by spin casting a drop of a solution mixture of 2.2×10^{-6} g/L dPPV-PPyV and 3 g/L polystyrene (Polysciences, $M_w \approx 50\,000$) in toluene onto a glass coverslip. A film thickness of ~30 nm was routinely obtained by this method of preparation. To reduce oxidative photobleaching, the sample coverslip was purged by nitrogen gas continuously during the experiments.

Single molecule images were acquired by a home-built sample-scanning confocal microscope based on a Zeiss Axiovert 135TV microscope and Topometrix scanning electronics. Raster scanning of the sample coverslip was achieved by an $X-Y$ scanning sample stage, which was driven by two electrostrictive actuators (Newport). The laser excitation was delivered to the epi-illumination port of the microscope by a single-mode optical fiber, which also served as a 3.3 μm wide spatial filter. The laser light that came out from the fiber was first collimated by an objective (Zeiss, CP-Achromat 5X), filtered through a narrow band interference filter, and then reflected up to a microscope objective (Zeiss, Achrostigmat 100X oil immersion 1.25 N.A.) by a dichroic beam splitter (Omega). The beam was chosen to completely fill the back of the microscope objective. Fluorescence from a single molecule collected by the same microscope objective was made to exit from the bottom of the microscope and allowed to focus onto a 200 μm aperture at the first image plane. This image was then relayed to a 100 μm pinhole via a combination of lenses and was finally focused onto an avalanche photodiode detector (APD) (EG&G Canada). Scattered laser light was removed by various combinations of notch (Kaiser) and long-pass colored glass filters. Emission spectra from single molecules were obtained by directing the fluorescence to a polychromator (Acton SpectraPro 150) equipped with a CCD camera (Princeton Instruments). To collect $I_{CW}(t)$ from a single molecule, a designated molecule chosen from an image scan was transported to the laser focus by the $X-Y$ scanning stage, and the emission intensity was continuously monitored by the APD at a preselected dwell time. The spot size of the sample molecules in the images was ~250 nm (the diffraction limit).

In a two-color excitation spectroscopy experiment, two independent excitation laser beams (488 and 514 nm for sulforhodamine G and 457 and 514 nm for dPPV-PPyV) were combined by a 50/50 beam splitter and coupled into the single-mode optical fiber that delivered the light to the epi-illumination port. The light intensity of each beam was "chopped" by an acoustic optic modulator (rise time, <1 μs) such that the molecule was continuously irradiated by one or the other of the two beams. The irradiation was switched (1 ms) from one color to the other at the beginning of each dwell period (1 ms). Separate scanning confocal imaging with each beam demonstrated that the focal spots of the beams were greater than 50% spatially overlapped at the location of the single molecule in the sample. The $I_{CW}(t)$ data were collected and sorted into two separated traces corresponding to the alternately chopped two-color excitation wavelengths.

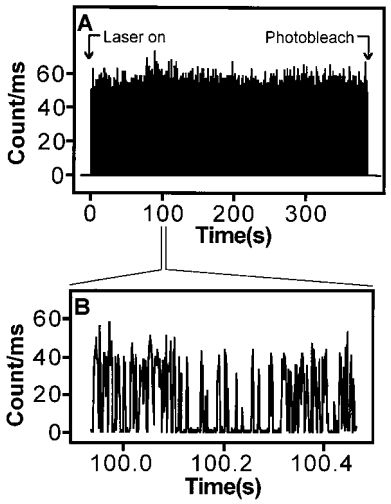

Figure 3. $I_{CW}(t)$ data of a single DiI molecule measured at 1 ms temporal resolution. $I_{CW}(t)$ in panel A shows up as a black block because of rapid blinking. Panel B is an expanded view of panel A near the 100th second.

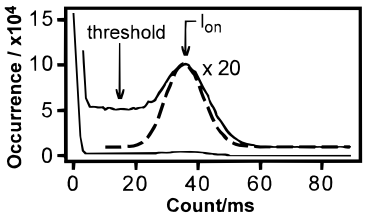

Figure 4. $H(I)$ obtained from the $I_{CW}(t)$ data in Figure 3A. For comparison, a Poisson distribution is plotted in a dashed line to represent the photon shot noise expected from a constant average fluorescence intensity of 36 counts/ms.

III. Results and Discussions

A. Triplet Blinking of DiI. Single molecule spectroscopy studies on DiI have revealed that intensity fluctuations of this single chromophoric molecule show clear evidence of triplet blinking.[27] In the present paper, we extensively explore the single molecule spectroscopy of DiI, emphasizing an intensity histogram analysis of $I_{CW}(t)$. The results are compared to stochastic simulations of $I_{CW}(t)$ based on a model that includes three electronic states (Figure 1) in order to determine to what extent triplet blinking alone, as opposed to additional processes, such as spectral diffusion, is responsible for the experimental behavior.

Figure 3 portrays the $I_{CW}(t)$ of a single DiI molecule on PMMA excited at 514 nm at an approximate excitation rate of 10^6 s^{-1}. The data show obvious intensity jumps from an average "on" intensity of ~36 counts/ms to an "off" intensity of ~0.3 counts/ms, which is the level of the background signal (scattered light and background fluorescence). As mentioned above, the "off" level of DiI has been previously assigned to a long-lived triplet state. Thus, the data are qualitatively consistent with the photophysical scheme outlined in Figure 1.

Figure 4 displays the $H(I)$ of the $I_{CW}(t)$ data shown in Figure 3. The intense feature in $H(I)$ that peaked at 0 counts/ms is due to the significant fraction of time that the molecule spends in the "off" level (T_1), while the broad peak near 36 counts/ms is due to the "on" level ($S_0 \leftrightarrow S_1$). The flat region of the histogram will be discussed below.

For a photodynamic model, such as Figure 1, the "blinking" kinetics can be characterized by compiling histograms of the duration of the "on" and "off" periods, respectively $H(t_{on})$ and $H(t_{off})$.[3,29] Parts A and B of Figure 5 show histograms of this type for DiI, which have been calculated from $I_{CW}(t)$ (Figure

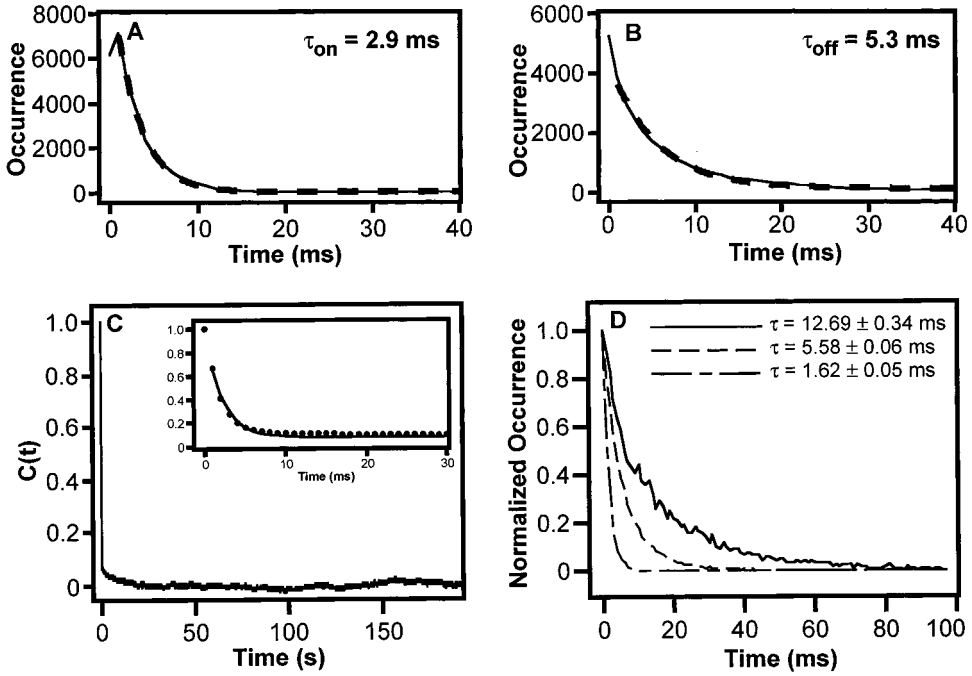

Figure 5. Calculated duration histograms and the $C_I(t)$ analysis of $I_{CW}(t)$. Panels A and B are the "on" and "off" duration histograms, respectively. The "on" and "off" intensity level was determined by the threshold level shown in Figure 4. Experimental data in both histograms are plotted as a solid line, whereas the dashed lines are obtained from a single-exponential fit. Panel C is the $C_I(t)$ of Figure 3A. The $C_I(t)$ at early time is shown in the inset. A biexponential fit to [1 ms to 30 s] is shown in solid line with 93% $\tau_1 = 2.3$ ms and 7% $\tau_2 = 9.3$ s. Panel D shows the "off" duration histogram of three molecules studied at different O_2/N_2 atmosphere.

3). The duration histogram analysis requires a somewhat arbitrary threshold level to distinguish between the "on" and "off" levels. The threshold level can be selected for example by choosing the threshold to be 1/2 of the peak intensity of the "on" level. However, the calculated duration histograms are not observed to be a strong function of the threshold choice if the chosen threshold lies in the flat region of $H(I)$. The $H(t_{off})$ is well fit by a single exponential with an average lifetime τ_{off} that is assigned to τ_{T_1}. $H(t_{on})$ is also well fit by a single exponential, and the average lifetime, τ_{on}, reflects the kinetics of T_1 formation (see Figure 1). It will be shown below that for single molecule systems that reveal continuous rather than discrete temporal intensity fluctuations, it is not possible to determine $H(t_{on})$ and $H(t_{off})$, since it is inappropriate to make an "on"/"off" level analysis.

As the sample is exposed to O_2/N_2 mixtures varying from pure N_2 to ambient air (80% partial pressure N_2), τ_{T_1} varies from as large as 19 ± 8 ms (samples in pure N_2) to much less than 1 ms (samples directly exposed to air) as shown in Figure 5D. (O_2 is widely known to induce $T_1 \rightarrow S_0$ intersystem crossing and enhance k_{isc}). Although the "off" duration histogram of each molecule that was studied is well fit by a single-exponential decay (e.g., $\tau_{T_1} = 5.3 \pm 0.2$ ms for Figure 5b), a significant distribution of τ_{T_1} is observed for different molecules under the same O_2/N_2 environment.

The excellent agreement between the expected behavior from a three-electronic-state model (Figure 1) and the experimentally observed behavior of single DiI molecules is demonstrated by comparing the experimental data to stochastic (Monte Carlo) simulations of $I_{CW}(t)$ and the corresponding histograms (Figure 6). The parameters required for the simulation include I_{on}, τ_{on}, and τ_{off}, which are defined in Figure 1. These parameters were readily identified with the experimental quantities extracted from Figure 5 parts A and B and the peak intensity of $H(I)$ in Figure 4.

An analysis of the simulated $I_{CW}(t)$ suggests that the intermediate flat region in $H(I)$ is due to on → off and off → on transitions that occur within a single "dwell time". The simulated $H(I)$ also shows that the width of the "off" peak and the "on" peak simply reflect the Poisson shot noise at these intensity levels. Thus, the experimental data of DiI are quantitatively consistent with the three-electronic-state model and show no apparent evidence of spectral diffusion or variations in other photodynamic parameters, e.g., τ_{T_1}, $\sigma(S_0 \rightarrow S_1)$, Φ_{Fl}. This is well supported by the single-exponential decays observed in both the "on" and "off" duration histograms and the effects of O_2 enhanced triplet quenching.

It is interesting to compare the duration histogram analysis of $I_{CW}(t)$ to the simpler and better known time autocorrelation function, $C_I(t)$, analysis of $I_{CW}(t)$, which is shown in Figure 5C and defined in a convenient normalized form as follows.

$$C_I(t) = \frac{\langle I_{CW}(0) I_{CW}(t)\rangle - \langle I_{CW}\rangle^2}{\langle I_{CW}{}^2\rangle - \langle I_{CW}\rangle^2} \tag{1}$$

Where $\langle I_{CW}\rangle$ is the mean intensity and $\langle I_{CW}{}^2\rangle$ is the mean of the square of the intensity. For the simple kinetic scheme in Figure 1, $C_I(t)$ has analogous information to the duration histogram analysis. As shown in eq 2, the "unormalized" autocorrelation function, $C_I'(t)$, is predicted to be a simple exponential plus a constant term.[30]

$$C_I'(t) = \langle I_{CW}(0) I_{CW}(t)\rangle \tag{2a}$$

$$C_I(t) = A + Be^{-t/\tau_{ac}} \tag{2b}$$

$$\frac{1}{\tau_{ac}} = \frac{1}{\tau_{on}} + \frac{1}{\tau_{off}} \tag{2c}$$

$$\frac{\tau_{on}}{\tau_{off}} = \frac{A}{B} \tag{2d}$$

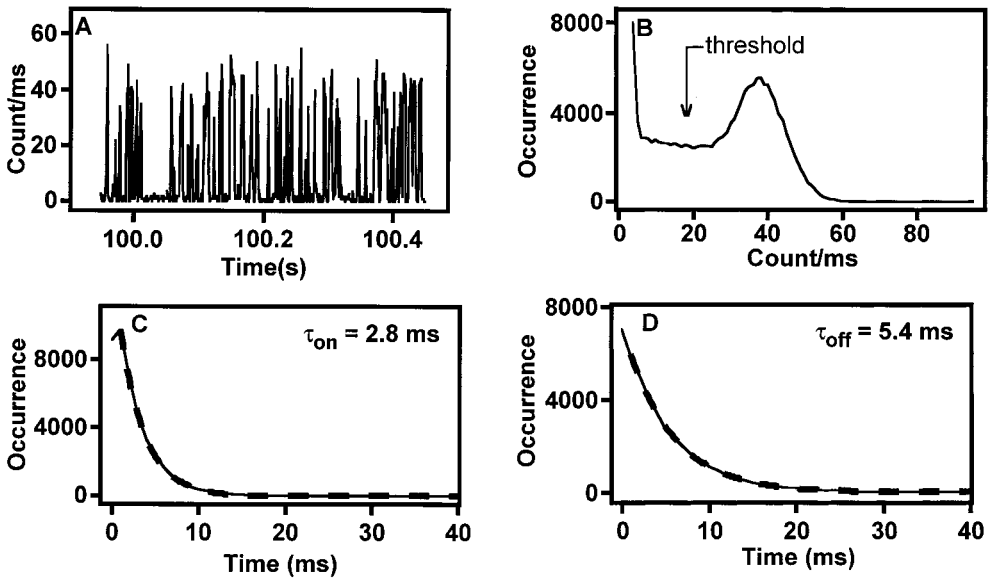

Figure 6. Monte Carlo simulation of $I_{CW}(t)$ based on the three-electronic-state model outlined in Figure 1. The parameters used for the simulation are $\tau_{on} = 2.0$ ms, $\tau_{off} = 5.2$ ms, $I_{on} = 39$ counts/ms. A portion of $I_{CW}(t)$ near the 100th second is shown in panel A. Panel B is the corresponding $H(I)$. The "on" and "off" duration histograms are calculated according to the threshold set in panel B and are shown in panels C and D, respectively. The simulated data are depicted by solid lines, while the dashed lines are obtained by a single-exponential fit.

TABLE 1: Comparison of the Duration Histogram Method and the Autocorrelation Method for Determining Rate Constants from an Analysis of $I_{CW}(t)$

analysis method	τ_{on}/ms	τ_{off}/ms
experimental $H(t_{on})$ and $H(t_{off})$	2.9	5.3
experimental $C_I(t)$	2.6	4.9
input to simulation	2.1	5.2
simulated $H(t_{on})$ and $H(t_{off})$	2.9	5.3
simulated $C_I(t)$	2.1	4.6

As summarized in Table 1, an autocorrelation analysis of experimental and simulated $I_{CW}(t)$ data for DiI leads to values for τ_{on} and τ_{off} that are within statistical error (~20%) of the corresponding values determined by the duration histogram method. $C_I(t)$ can also be applied to single molecule systems with continuous rather than discrete temporal intensity fluctuations. For such systems, however, eq 2 is not appropriate, since it is based on a kinetic model with discrete chemical species, i.e., T_1, S_1, S_0.

For more complex kinetic schemes, involving more kinetic intermediates, $C_I(t)$ has considerably less information than the separate "on" and "off" duration histogram, which uniquely assigns the kinetic parameters to the "on" and "off" processes. In addition, it should be emphasized that an autocorrelation analysis alone leads to very little information on the nature of the underlying dynamics. For example, blinking or spectral diffusion leads to essentially the same form of $C_I(t)$. In contrast, an examination of $H(I)$ can distinguish between these processes; see below.

The autocorrelation analysis does however offer a convenient framework for quantitatively examining the intensity fluctuations. The starting point is the total variance, σ^2 of the intensity fluctuations

$$\sigma^2 = \langle I_{CW}{}^2 \rangle - \langle I_{CW} \rangle^2 \tag{3}$$

For single molecules, a significant component of the total variance is usually associated with fast processes that occur on a time scale much shorter than the dwell time (t_{dw}) of the measurements (in the present case 1 ms). In terms of $C_I(0)$, the fast component of the variance is given by

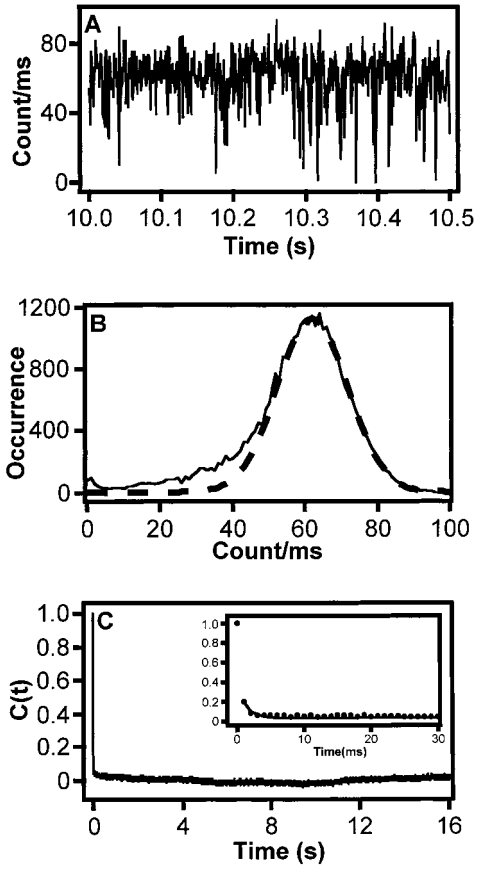

Figure 7. Expanded view of $I_{CW}(t)$ near the 10th second of a DiI molecule at high O_2 concentration is shown in Panel A. Panel B is the corresponding $H(I)$. The solid line is the experimental data, and the dashed line is obtained from a Gaussian fit to [61−100 counts/ms]. The $C_I(t)$ of the data shown in panel A is displayed in panel C. The first spike in $C_I(t)$ accounts for 80% of $C_I(t)$ in which 28% is photon shot noise and 52% is due to rapid fluctuations including unresolved blinking. The inset shows the early time behavior of $C_I(t)$.

$$\sigma_{fast}{}^2 = \sigma^2(C_I(0) - C_I(t_{dw})) \tag{4}$$

For the observed $I_{CW}(t)$ data (Figure 5C), $\sigma_{fast}{}^2 = 74.2$, which includes a 13% component due to photon shot noise ($\sigma_{PN}{}^2 =$

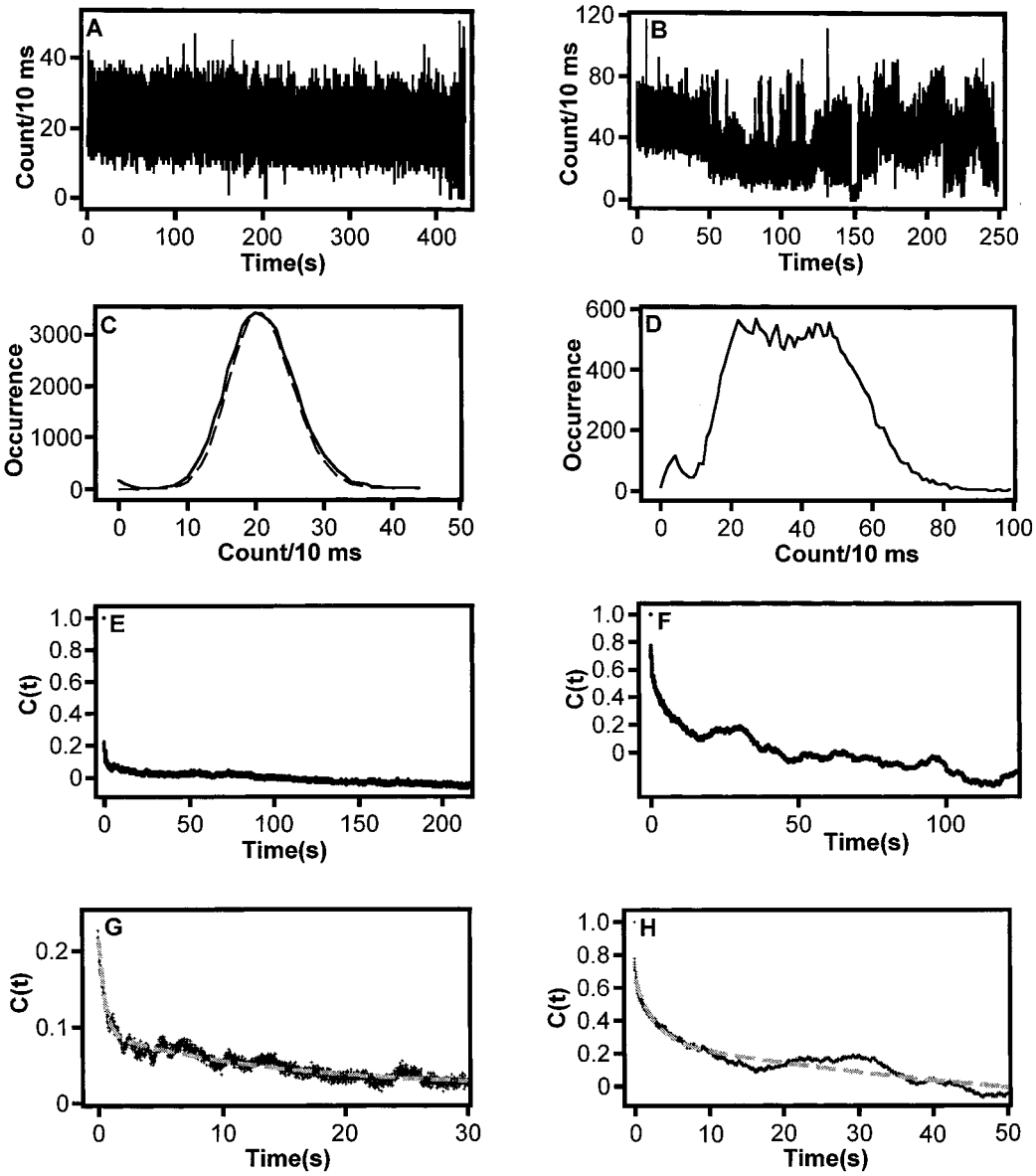

Figure 8. $I_{CW}(t)$, $H(I)$, and $C_I(t)$ analysis of two different sulforhodamine G molecules. The results are grouped into panels A, C, E, and G for one molecule and panels B, D, F, and H for the other. Panels A and B show the $I_{CW}(t)$ data. The corresponding $H(I)$ are shown in panels C and D. For comparison, the dashed line drawn in panel C is a Poisson distribution centered at 21 counts/10 ms. Panels E and F display the $C_I(t)$ of the two molecules. Panels G and H show the early time portion of $C_I(t)$. In panel G, the dashed line is a biexponential fit to [10 ms to 50 s] with 64% τ_1 = 0.5 s and 36% τ_2 = 14.0 s. The biexponential fit to [10 ms to 50 s] in panel H gives 38% τ_1 = 2.6 s and 62% τ_2 = 81 s.

$\langle I_{CW} \rangle \approx 9.8$ counts^2) and a much larger component (87%) due to unresolved blinking. (The instrumental noise due to laser intensity fluctuations, optical fiber coupler noise, etc. is less than 5% of $\langle I_{CW} \rangle$ and is considerably smaller than the observed fluctuations.) An analogous analysis of the simulated data support these conclusions.

It is interesting to consider the manifestations of triplet blinking at high O_2 concentrations where τ_{T_1} becomes much less than the 1 ms dwell time. The large intensity fluctuations (downward spikes) in Figure 7 are due to T_1 states that are formed *and* relaxed within a single dwell time. As a result, $H(I)$ in Figure 7B does not exhibit an intense peak at the background level as opposed to that shown in Figure 4. The peak in Figure 7B is compared to a Gaussian distribution that contains only 9% more broadening (fwhm) beyond the estimated photon shot noise. However, the extreme asymmetry of the peak toward the background level is a clear indication of unresolved triplet blinking. Indeed, the $C_I(t)$ analysis of $I_{CW}(t)$ collected under high O_2 concentrations clearly shows a large initial drop (80%), which is due predominantly to unresolved blinking.

B. Spectral Diffusion of Sulforhodamine G. Recently Xie and co-workers have studied spectral diffusion of sulforhodamine 101 dye by single molecule spectroscopy.[15] In this paper, we present similar findings on the related compound sulforhodamine G (Figure 8). We have studied $I_{CW}(t)$ of this compound at an excitation close to the red edge of its absorption spectrum. The data exhibit intensity fluctuations that occur over a broad distribution of time scale and are much larger than the photon shot noise. Occasionally, the time scale of the slowest fluctuation is too slow to achieve a statistical distribution within the survival time of a single molecule. As a result, $H(I)$ and $C_I(t)$ calculated from different long segments of $I_{CW}(t)$ from some molecules show significant variations due to insufficient sampling. In general, individual molecules show extremely different fluctuation amplitudes and time scale.

For the first molecule in Figure 8 (four panels on the left-hand side), an analysis of $H(I)$ and $C_I(t)$ reveals that the fast intensity fluctuations are dominated by photon shot noise. At longer times, two additional process are observed in $C_I(t)$ with exponential relaxation times of ~0.5 and ~14 s. For the other molecule portrayed in Figure 8, large-amplitude fluctuations with relaxation times ranging from ~2.6 s to greater than 80 s are apparent. The longer time scale process is not, however, well-sampled during the 120 s lifetime of the molecule.

The general behavior of $H(I)$ and the $C_I(t)$ analysis of the sulforhodamine G molecules that we have investigated reflects the underlying spectral diffusion exhibited by this class of molecules.[15] This is nicely demonstrated by the symmetric peak located at the average emission intensity in $H(I)$ in conjunction with the $C_I(t)$ analysis of sulforhodamine G that shows substantial contributions from resolvable decay components carrying significant amplitudes. The intensity distributions in $H(I)$ is significantly broader than the Poisson shot noise at both high and low intensity levels. Since these processes produce a symmetrical Gaussian broadening in $H(I)$, the data are more consistent with spectral diffusion than photophysical blinking. In fact, since only one peak is apparent in $H(I)$, it is not appropriate to use a duration analysis for this example.

The time constants for the $C_I(t)$ decay components are in qualitative agreement with the analogous study of the S_1-S_0 energy gap autocorrelation, $C_\nu(t)$, of sulforhodamine 101.[15]

$$C_\nu(t) = \langle \nu(0)\nu(t)\rangle - \langle \nu\rangle^2 \qquad (5)$$

where $\nu(t)$, the instantaneous spectral mean of the fluorescence, was obtained from time- and wavelength-resolved single molecule fluorescence spectra. Thus, the intensity fluctuations in $I_{CW}(t)$ of sulforhodamine G are apparently associated with dynamics that lead to spectral diffusion. This is consistent with the observation by Lu and Xie that the fluctuations in $I_{CW}(t)$ of sulforhodamine 101 are strongly correlated with the fluctuations of $\nu(t)$.[15] As mentioned above, this is believed to be the result of spectral fluctuations in the absorption spectrum and, consequently, the single molecule excitation rate.

The effects of spectral diffusion on the excitation rate of sulforhodamine G are further demonstrated in Figure 9. These $I_{CW}(t)$ data were acquired by two-color excitation spectroscopy in which two excitation wavelengths at a single molecule were rapidly switched. The $I_{CW}(t)$ data were collected in synchronous with the switching wavelengths and sorted into two separated traces accordingly. Each trace was then binned to an effective dwell time of 100 ms and gave $I_{CW}(t)$ at the corresponding excitation wavelength. The purpose of this experiment is to yield excitation wavelength resolved single molecule fluorescence data. The two sorted and binned $I_{CW}(t)$ data sets are nearly simultaneously collected from a single molecule at two different excitation wavelengths (Figure 9 parts A and B). Thus, the data lead to direct observations of spectral diffusion without the extreme loss of signal-to-noise that is inherent to emission wavelength resolved measurements.

A comparison of the emission intensity induced by 488 and 514 nm excitation and the ratio of these intensities (Figure 9C) suggests that there are dramatic intensity fluctuations due to a time-dependent shift in the absorption spectrum, i.e., spectral diffusion. Moreover, the magnitudes of the fluctuation are bigger at 514 nm excitation. The 514 nm excitation wavelength is closer to the red-edge of the absorption spectrum, where spectral diffusion should have the biggest effect on the excitation cross sections. In contrast, 488 nm is closer to the peak of the absorption spectrum, where spectral diffusion is expected to have

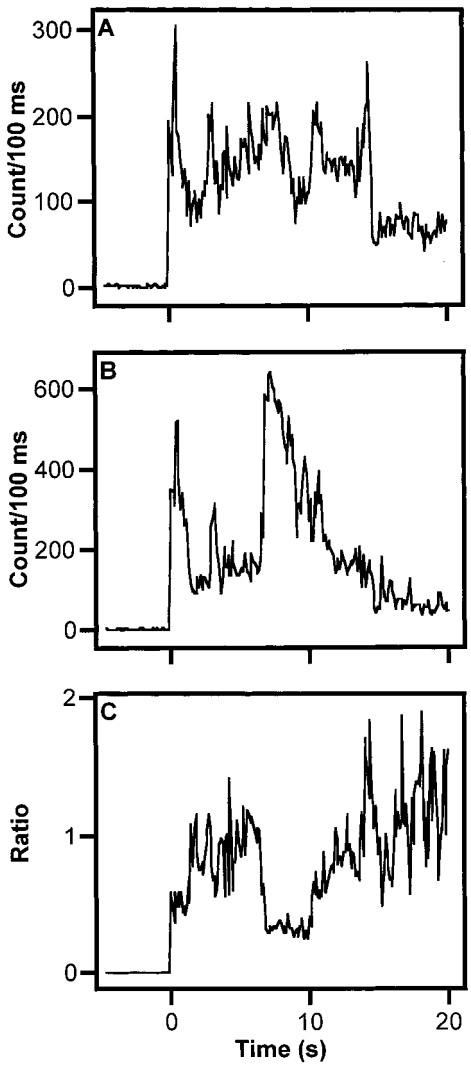

Figure 9. The $I_{CW}(t)$ data of a sulforhodamine G molecule obtained from two-color excitation spectroscopy. Panel A shows the $I_{CW}(t)$ obtained by 488 nm excitation, whereas panel B shows the simultaneously collected $I_{CW}(t)$ data with 514 nm excitation. Panel C is the intensity ratio of the 488 nm $I_{CW}(t)$ to the 514 nm $I_{CW}(t)$.

minimal impact on the excitation cross sections. All sulforhodamine molecules investigated by the two-color excitation showed some evidence of spectral diffusion, but the effect is generally less obvious than that shown in Figure 9. It is not known whether the variation from molecule to molecule was due to an inhomogeneous environmental distribution or an insufficient sampling time due to photobleaching.

C. Multichromophoric Molecules and Assemblies. Single molecule spectroscopy of isolated multichromophoric molecules/assemblies, including conjugated polymer molecules,[13] photosynthetic light-harvesting complexes LH2,[14] semiconductor nanocrystals,[31] and other biomolecules,[19] is leading to new insight into the photophysics and photochemistry of this class of multichromophoric molecules/assemblies. In this paper, we examine several aspects of the intensity fluctuation of such systems. A simple, simulated example of how intensity fluctuations of individual molecules are "masked" in a multichromophoric system is given in Figure 10. A simulated $I_{CW}(t)$ for 500 excited DiI molecules and the associated $H(I)$ are shown in Figure 10 parts A and B, respectively. The simulation was accomplished by adding together 500 replicas of the $I_{CW}(t)$ data in Figure 3A with random time delays and a $\sin^2\theta$ distribution of excitation rates to account for the randomness

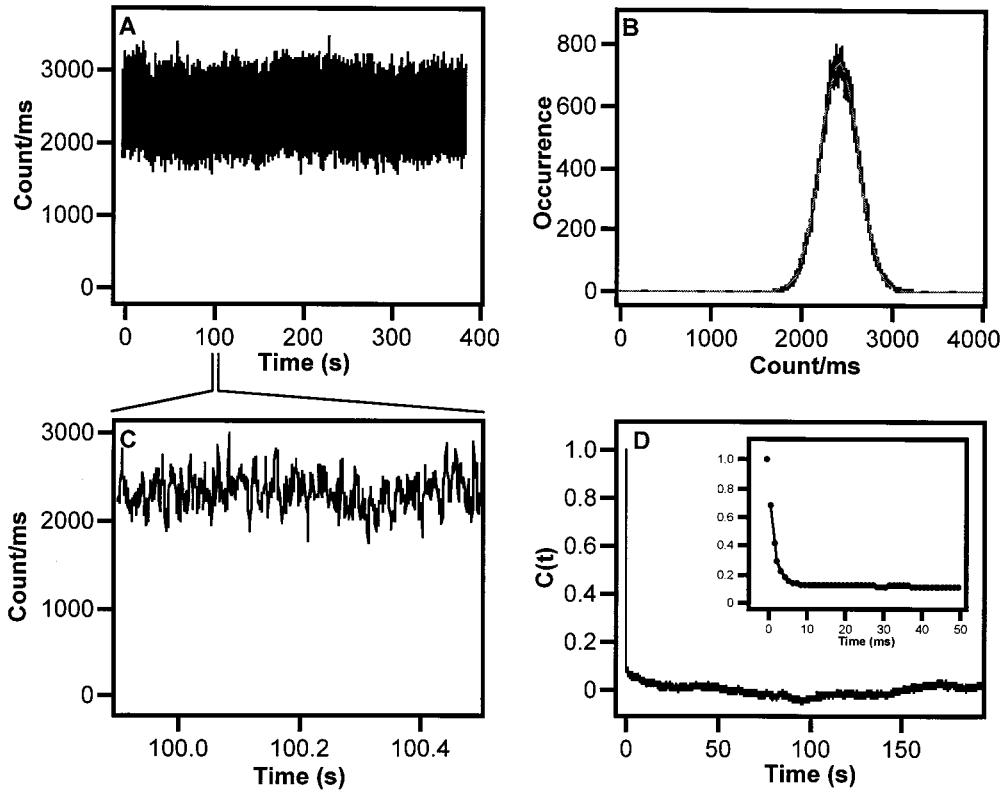

Figure 10. $I_{CW}(t)$, $H(I)$, and $C_I(t)$ analysis of the sum of 500 replicas of Figure 3A. The dashed line is a Gaussian fit with $\sigma = 207$ counts/ms. Panel C displays an expanded view of the $I_{CW}(t)$ shown in panel A. The complete and the early portion of $C_I(t)$ are shown in panel D and the inset, respectively.

of the polar angle θ. Parts A and C of Figure 10 nicely demonstrate the well-known result that statistical averaging in multichromophoric systems significantly diminishes intensity fluctuations due to individual chromophores. This is well understood in the context of fluorescence correlation spectroscopy.[32]

A related actual example of a multichromophoric system is a dye-doped polymer bead. For example, the data shown in Figure 11 correspond to ~180 weakly interacting dye molecules imbedded in a single 20 nm polymer bead. The average separation between dye molecules in the polymer bead is 32 Å. At low excitation power (200 W cm^{-2}), the fluorescence from a single dye-label sphere shows no evidence of photobleaching after hundreds of seconds of irradiation. The $I_{CW}(t)$ data of the sphere (Figure 11) display instantaneous fluctuations due predominately to photon shot noise. The $H(I)$ in Figure 11B exhibits no evidence of blinking or spectral diffusion. It is important to emphasize, however, that the absence of blinking in the data may be a consequence of statistical averaging among the ~180 chromophores as described in the previous paragraph.

In striking contrast to the behavior of the two model systems, it was recently reported that the multichromophoric conjugated polymer dPPV-PPyV exhibits extremely large single molecule intensity fluctuations.[13] The $I_{CW}(t)$ data of four conjugated polymer molecules shown in Figure 12 reveal large-amplitude discrete intensity jumps, which we recently attributed to rapid changes in the fluorescence quantum yield of the molecule.[13] Alternative explanations for these discrete intensity jumps including spectral diffusion of the absorption spectrum and/or the instantaneous loss of absorption due to the population of a nonabsorbing "dark" state were argued to be less likely. In particular, the rapid decreases in fluorescence intensity were assigned to efficient intramolecular electronic energy transfer along the 1-D polymer chain to a photogenerated localized

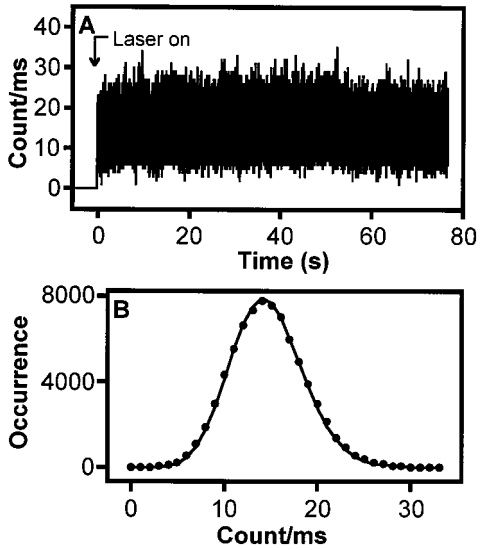

Figure 11. Panel A shows the $I_{CW}(t)$ of a 20 nm fluorescent microsphere (Molecular Probe, F-8787) measured at 1 ms temporal resolution. The $I_{CW}(t)$ seldom drops to the background level. Panel B shows the corresponding $H(I)$ together with a Poisson distribution drawn as a solid line for comparison. The mean of the Poisson distribution is 14.6 counts/ms. Intensity fluctuations are mostly due to Poisson shot noise, which accounts for 99% of the first spike or 93% of $C_I(t)$.

excitation-quenching polymer defect. In the present paper, we describe the evidence for this interpretation in more detail.

The dPPV-PPyV polymer under investigation in this paper has a molecular weight of ~22,000. This corresponds to ~20 monomer units, which can extend to as long as ~50 nm. According to the usual spectroscopic models for conjugated polymers, a polymer of this size would have multiple conjugated segments, implying that the system is effectively multichro-

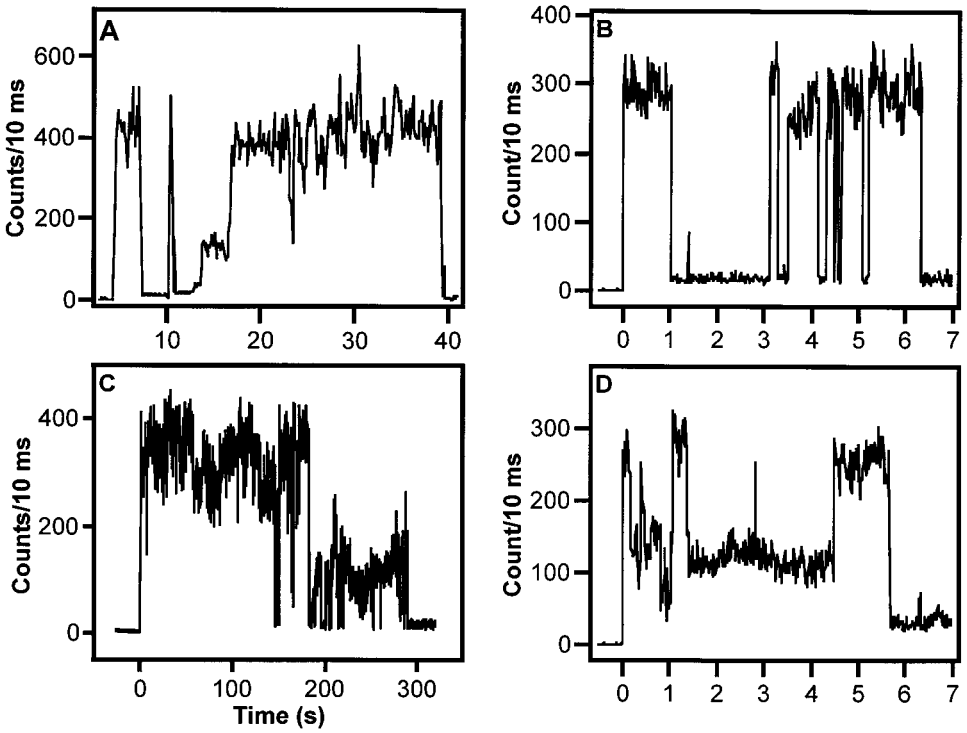

Figure 12. $I_{CW}(t)$ of four dPPV-PPyV single molecules at 10 ms temporal resolution. Each $I_{CW}(t)$ exhibits distinctive intensity jumps during the lifetime of the molecule.

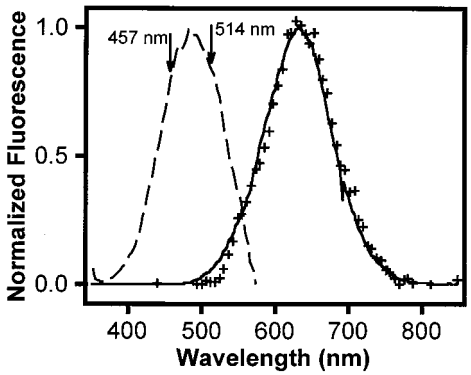

Figure 13. Absorption and fluorescence spectra of dPPV-PPyV. Dashed line denotes the thin film absorption spectrum. The solid line and the crosses show the fluorescence spectra from a thin film sample and a single dPPV-PPyV molecule, respectively. All emission spectra are obtained by 488 nm excitation.

mophoric. Accordingly, the absorption spectrum of the polymer is due to overlapping absorption bands from different conjugated segments of the polymer chain. In contrast, the emission (Figure 13) may be due to emission from a small fraction of the total polymer chain, specifically the regions that correspond to local minima in the optical band structure. By analogy to other conjugated polymers, these regions should be efficiently populated on a picosecond time scale by intramolecular electronic energy transfer.[33−35]

The $H(I)$ data for individual dPPV-PPyV molecules reveal a highly diverse behavior (Figure 14). Nevertheless, an obvious peak in $H(I)$ is observed at the background level in all cases. Thus, the $H(I)$ data suggest that the conjugated polymer reversibly changes into a "dark" form in which either the absorption cross section at the excitation wavelength or the fluorescence quantum yield of the "dark" polymer is orders of magnitude smaller than its emitting counterpart. In addition to the background peak, the $H(I)$ data of individual molecules also reveal extra peaks corresponding to different emitting forms of the polymer. In all cases, the highest intensity peak in $H(I)$ corresponds to the average intensity level of the polymer immediately after it is irradiated. Thus, the lower intensity peaks and the peak at the background level arguably correspond to polymer molecules that had been irradiated for an extended period of time.

While many dPPV-PPyV molecules seem to reveal two intensity peaks in $H(I)$, as shown in Figure 14A, few molecules exhibit three and occasionally four intensity peaks (Figure 14 parts B and C). It should be emphasized that the lifetimes of most molecules are short relative to some long time scale intensity fluctuations and make it impossible to construct a statistically meaningful $H(I)$. In particular, while an examination of the $I_{CW}(t)$ data reveals that most molecules reversibly "visit" high and low intensity levels, a histogram of the early and late time segment of the $I_{CW}(t)$ data leads to noticeably different results. In an attempt to determine a statistically meaningful $H(I)$, we have constructed a grand histogram by adding together the intensity histograms from 63 molecules. To normalize the data, the individual histograms were normalized to the average intensity in the first second of the $I_{CW}(t)$ data. The grand histogram is shown in Figure 14D. It should be emphasized that this histogram is statistically meaningful. This was demonstrated by taking different subsets from the 63 molecules studied and showing that a nearly identical histogram was observed for each subset of molecules chosen from the ensemble. Furthermore, the grand histogram is also not a strong function of the time segment that is sampled during the lifetime of the various molecules. The three peaks shown in the grand histogram suggest at least three intensity levels exist in the conjugated polymer molecules.

In an attempt to determine whether the intensity fluctuations portrayed in Figure 12 were a simple result of spectral diffusion, we undertook an investigation of the $I_{CW}(t)$ data for the conjugated polymer with two-color excitation spectroscopy. As previously described, these data, which are reproduced in Figure 15, clearly demonstrated that the intensity fluctuations in the

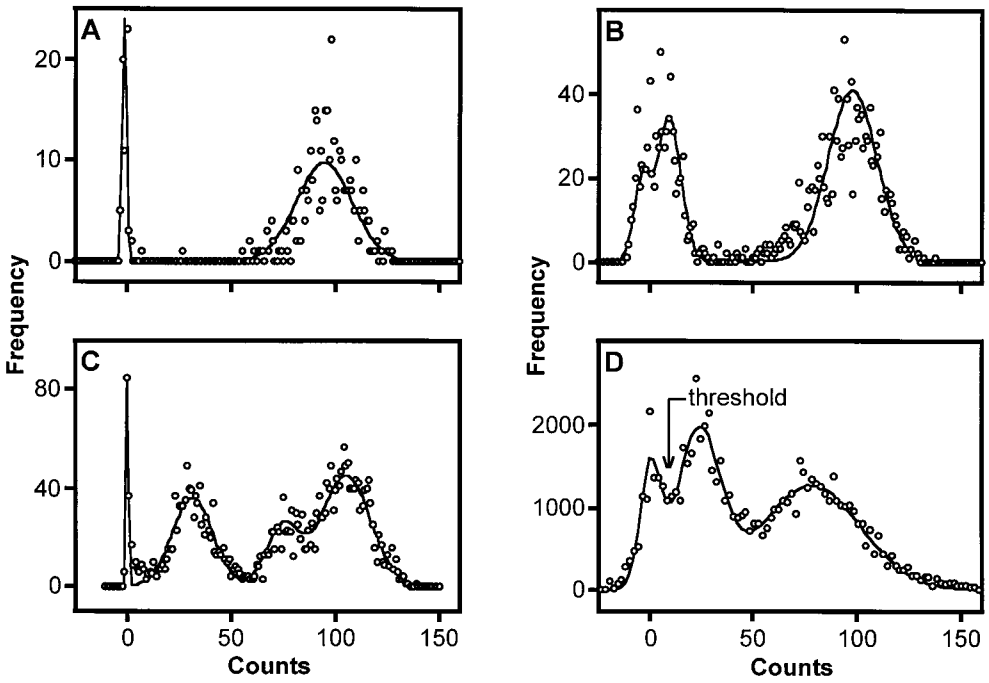

Figure 14. $H(I)$ data of single dPPV-PPyV molecules. The $H(I)$ data in panels A, B, and C are obtained from three single molecules, showing the possible number of emitting state in each molecule. Panel D shows the grand intensity histogram constructed from 63 single dPPV-PPyV molecules. In all panels, the circles are experimental data and the solid lines are Gaussian fits.

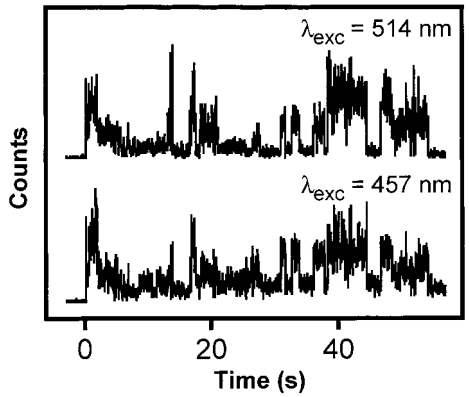

Figure 15. Two-color excitation spectroscopy of dPPV-PPyV. The upper traces shows the $I_{CW}(t)$ obtained with 514 nm excitation. The lower trace is the $I_{CW}(t)$ data obtained almost simultaneously from the same molecule with 457 nm excitation.

conjugated polymer are not a result of spectral diffusion since nearly simultaneous excitation at two very different excitation wavelengths leads to similar intensity fluctuations. Indeed, the high degree of correlation between the two $I_{CW}(t)$ data sets, especially those relatively small changes in the fluorescence intensity, strongly suggests that the fluorescence intensity fluctuations originate from very complex behavior of the single polymer molecule, which is certainly oversimplified by the apparent three-intensity-level model implied by the grand histogram shown in Figure 14D.

It is unlikely that the intensity blinking is due to quenching by localized "Frenkel" triplet excitons, since these typically have (for conjugated polymers) a much shorter lifetime (<10 ms) than the observed lifetime of the dark state (~200 ms). The quencher responsible for the dark state may however be a triplet and/or singlet separated radical ion pair along the polymer chain.

A simple model that can roughly account for the reversible intensity fluctuations of the conjugated polymer is outlined in Figure 16. During the emitting periods of the $I_{CW}(t)$ data, the polymer molecule is apparently well represented by the form

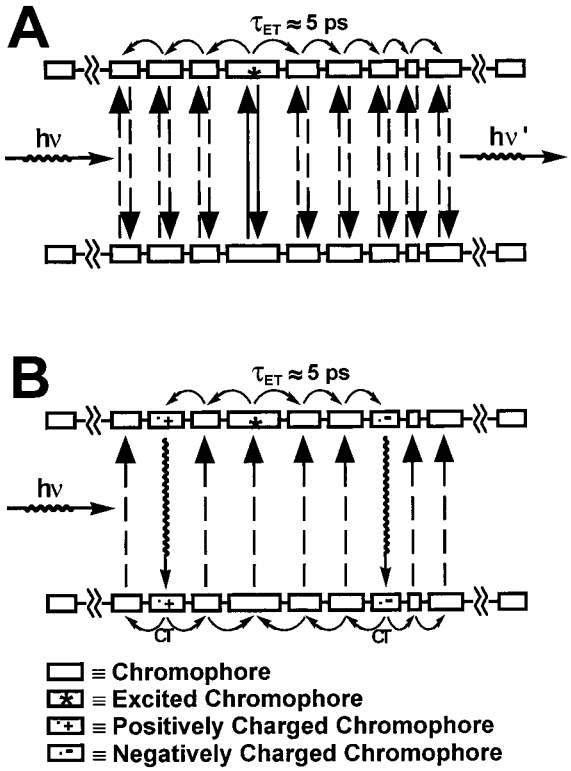

Figure 16. Simple model for the photophysics of a single dPPV-PPyV molecule.

pictured in Figure 16A. In this form of the polymer, random excitations along the polymer backbone lead to rapid intramolecular electronic energy transfer to one or more minima in the optical band structure of the polymer. For each excitation period, the original excitation that is denoted by the asterisk in Figure 16A can migrate rapidly along the polymer backbone and emit from any conjugated segment (a chromophore) of the polymer with which a local minimum is associated. In contrast, the nonemitting form of the polymer in Figure 16B is ascribed

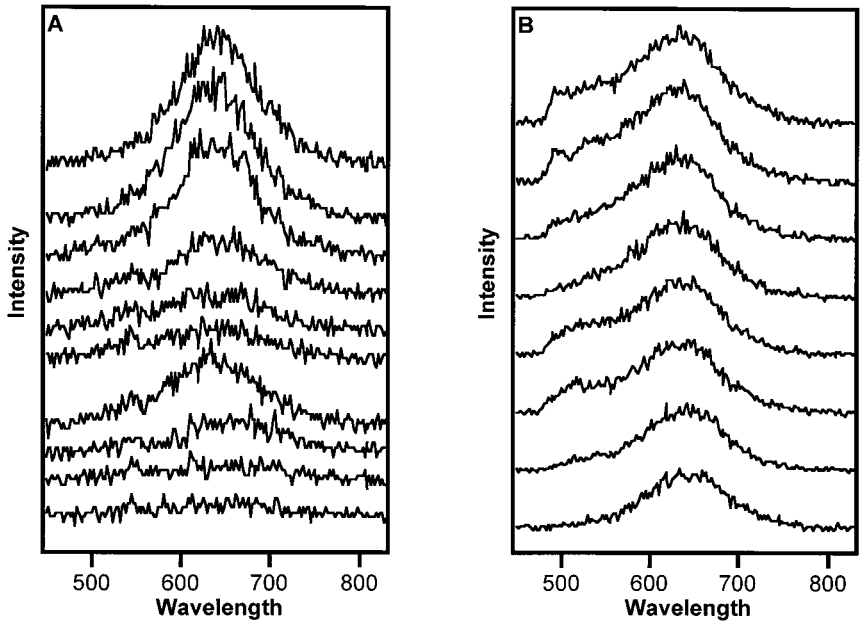

Figure 17. Single molecule fluorescence spectra of dPPV-PPyV taken at 20 s consecutive intervals.

to a photochemically modified version of the polymer in which continuous excitation leads to charge separation via a low quantum yield process.[36,37] Charge separation produces radical cation and radical anion defects that are expected to efficiently quench subsequent singlet excitations along the polymer chain *by a charge-transfer mechanism*.[38] It is also very likely that charge separation occurs in the vicinity of the local minima where most initial excitations will terminate. In fact, these ionic defects may actually locate exactly at the local minima of the polymer molecule. If the optical band structure is not strongly affected by the generation of the polymer defects, it would continue to direct excitations toward the local minima (now become the defects). Thus, the defects located at the minima of the optical band structure would diminish the fluorescence quantum yield of the polymer molecule as a result of efficient intramolecular electronic energy transfer of singlet excitations to the defect sites followed by efficient quenching.

At this point, it is clear that the model implied in Figure 16 is at best an oversimplification of the complex behavior of real polymer systems. For example, such a simplified model does not suggest an interpretation for the multiple intensity peaks in $H(I)$. Indeed, the model outlined in Figure 16 would suggest that the polymer has only two emitting forms, an "on" state, when no photogenerated defects are found, and an "off" state, when there exists one or more defects (e.g., cation/anion pair) in the polymer molecule. Although it is possible to argue that intermediate emitting levels may be due to the emission from conjugated segments with different fluorescence quantum yields, it is unlikely that a ~50 nm dPPV-PPyV molecule contains only a few conjugated segments as implied by the grand histogram. The presence of an intermediate emitting level may also be the result of two different types of polymer defects with one being a highly efficient excitation quencher and the other being less effective, which leads to the intermediate intensity peak. But more research will be necessary to adequately address this possibility.

The fluorescence spectra as a function of time during the lifetime of a polymer molecule lead to further insight into the quenching process. Most molecules exhibit the behavior shown in Figure 17A. The fluorescence spectrum stays constant in shape during the polymer lifetime, but when the fluorescence intensity blinks "off" and "on", so does the fluorescence spectrum. The data in Figure 17 are not of sufficient temporal resolution to show the actual "off" periods as in the $I_{CW}(t)$ data, but the fluorescence intensity fluctuations manifest themselves as changes in the integrated area under the fluorescence peak. Figure 17B shows a rare but significantly different behavior for a few polymer molecules where two distinct emission regions are apparent. One region of emission covers the same 650 nm spectral region as that seen in Figure 17A, whereas the other region is at a significantly shorter wavelength and in fact is distorted on the blue edge by the filters in the collection optics of the microscope. The two regions of emission reveal very different intensity fluctuations. In fact, the fluorescence intensity of each spectral region appears to fluctuate independently. Thus, for these rare molecules, there is strong evidence that there are two independent regions of emission that can give rise to intermediate intensity levels in the $I_{CW}(t)$ data.

In a previous paper,[13] we have shown how "on" and "off" duration histograms can be constructed for the conjugated polymer molecule dPPV-PPyV by arbitrarily setting the threshold at the value shown in Figure 14D. These data show for an ensemble of single molecules and a few relatively long-lived single molecules that the on → off transition is a result of photoexcitation. In other words, the rate of transition from the "on" to the "off" state increases monotonically with the excitation rate. On the contrary, the off → on transition is independent of the excitation rate and presumably results from a thermally driven process. A candidate for the off → on transition consistent with the model in Figure 16 would be the thermally induced reverse electron transfer between the radical cation and radical anion defects along the polymer chain.

It should be emphasized that while the three-intensity-level model implied by the grand intensity histogram is certainly too primitive to describe the very complex intensity fluctuations of the conjugated polymer, it nevertheless suggests that the intensity fluctuations occur with discrete intensity jumps rather than continuous fluctuations of the fluorescence intensity. Thus, consecutive fluorescence photobleaching and/or blinking of independent chromophoric regions along the polymer chain can be ruled out by the dramatic and discrete jumps in fluorescence intensity observed in these measurements. In particular, the

dramatic and discrete jumps in fluorescence intensity strongly suggest a cooperative behavior of the different conjugated segments of the polymer. In the model outlined in Figure 16, the cooperative behavior is the result of intramolecular electronic energy transfer that effectively links all conjugated segments of the polymer together. This suggests a general mechanism for fluorescence intensity fluctuations in conjugated polymer molecules, since efficient intramolecular electronic energy transfer should be a common feature for such systems. We have recently investigated the single molecule spectroscopy of the well-known conjugated polymer poly[2-methoxy,5-(2′-ethylhexoxy)-*p*-phenylenevinylene] (MEH-PPV). Very large fluorescence intensity jumps are observed for MEH-PPV in analogous fashion to that of dPPV-PPyV. However, for the much larger MEH-PPV polymer molecule ($M_w \approx 1\,000\,000$), the fluorescence intensity fluctuations do not occur to the background level. Thus, in a larger polymer, intramolecular electronic energy transfer is not efficient enough to connect all conjugated segments of a polymer molecule together. A single polymer defect in MEH-PPV does not have the same dramatic effect on the fluorescence quantum yield observed in dPPV-PPyV. This is consistent with the much longer length of greater than 3 μm for the MEH−PPV molecules under investigation.

IV. Conclusions

The single molecule spectroscopy of a diverse set of single-chromophoric dye molecules and multichromophoric systems has been investigated. For each system, the transient emission $I_{CW}(t)$ data has been obtained with CW irradiation. The intensity histogram of $I_{CW}(t)$ leads to characteristic behavior for each system that can be interpreted in terms of certain key photophysical behaviors such as blinking due to triplet bottlenecks, spectral diffusion due to environmental fluctuations, and more complex phenomena involving blinking due to efficient intramolecular electronic energy transfer and subsequent quenching by a photogenerated quencher. The classification of the photophysical behavior of each particular system is supported by other types of single molecule spectroscopic data including two-color excitation spectroscopy, wavelength-resolved single molecule fluorescence spectroscopy, and the dependence of these data on variations of the excitation power density.

The result on the simple single-chromophoric dye molecules leads to clear interpretations of the various types of single molecule data and helps formulate some simple procedures for classifying photophysical dynamics of molecules by single molecule spectroscopy. Application of such procedures to the single molecule spectroscopy of more complex systems, such as the conjugated polymer dPPV-PPyV molecule, leads to further evidence that the dramatic intensity fluctuations of the conjugated polymer are due to efficient intramolecular electronic energy transfer with subsequent excitation quenching by photogenerated quenchers along the polymer chain.

Acknowledgment. This work was supported by the National Science Foundation and the University of Minnesota. We thank T. A. Swager and D.-K. Fu for supplying the sample of dPPV-PPyV that was studied in this paper.

References and Notes

(1) Single Molecules and Atoms. *Acc. Chem. Res.* **1996**, *29* (12).
(2) *Single Molecule Optical Detection, Imaging, and Spectroscopy*; Basche, T., Moerner, W. E., Orrit, M., Wild, U. P., Eds.; Verlag Chemie: Munich, 1996.
(3) Moerner, W. E.; Basche, T. *Angew. Chem., Int. Ed. Engl.* **1993**, *32*, 457.
(4) Xie, X. S.; Dunn, R. C. *Science* **1994**, *265*, 361.
(5) Trautman, J. K.; Macklin, J. J.; Brus, L. E.; Betzig, E. *Nature* **1994**, *369*, 40.
(6) Macklin, J. J.; Trautman, J. K.; Harris, T. D.; Brus, L. E. *Science* **1996**, *272*, 255.
(7) Dickson, R. M.; Norris, D. J.; Tzeng, Y. L.; Moerner, W. E. *Science* **1996**, *274*, 966.
(8) Funatsu, T.; Harada, Y.; Tokunaga, M.; Saito, K.; Yanagida, T. *Nature* **1995**, *374*, 555.
(9) Jia, Y. W.; Sytnik, A.; Li, L. Q.; Vladimirov, S.; Cooperman, B. S.; Hochstrasser, R. M. *Proc. Natl. Acad. Sci. U.S.A.* **1997**, *94*, 7932.
(10) Schmidt, T.; Schutz, G. J.; Baumgartner, W.; Gruber, H. J.; Schindler, H. *J. Phys. Chem.* **1995**, *99*, 17662.
(11) Schmidt, T.; Schutz, G. J.; Baumgartner, W.; Gruber, H. J.; Schindler, H. *Proc. Natl. Acad. Sci. U.S.A.* **1996**, *93*, 2926.
(12) Ha, T.; Enderle, T.; Chemla, D. S.; Selvin, P. R.; Weiss, S. *Phys. Rev. Lett.* **1996**, *77*, 3979.
(13) Vanden Bout, D. A.; Yip, W. T.; Hu, D. H.; Fu, D. K.; Swager, T. M.; Barbara, P. F. *Science* **1997**, *277*, 1074.
(14) Bopp, M. A.; Jia, Y.; Li, L.; Cogdell, R. J.; Hochstrasser, R. M. *Proc. Natl. Acad. Sci. U.S.A.* **1997**, *94*, 10630.
(15) Lu, H. P.; Xie, X. S. *Nature* **1997**, *385*, 143.
(16) Basche, T.; Tittel, J.; Kettner, R.; Brauchle, C.; Quante, H.; Mullen, K. *J. Lumin.* **1995**, *64*, 1.
(17) Moerner, W. E. *Science* **1994**, *265*, 46.
(18) Ha, T.; Enderle, T.; Ogletree, D. F.; Chemla, D. S.; Selvin, P. R.; Weiss, S. *Proc. Natl. Acad. Sci. U.S.A.* **1996**, *93*, 6264.
(19) Wu, M.; Goodwin, P. M.; Ambrose, W. P.; Keller, R. A. *J. Phys. Chem.* **1996**, *100*, 17406.
(20) Ha, T.; Enderle, T.; Chemla, D. S.; Selvin, P. R.; Weiss, S. *Chem. Phys. Lett.* **1997**, *271*, 1.
(21) Dickson, R. M.; Cubitt, A. B.; Tsien, R. Y.; Moerner, W. E. *Nature* **1997**, *388*, 355.
(22) Tietz, C.; Daum, R.; Drabenstedt, A.; Schuster, J.; Fleury, L.; Gruber, A.; Wrachtrup, J.; Vonborczyskowski, C. *Chem. Phys. Lett.* **1998**, *282*, 164.
(23) Basche, T.; Moerner, W. E.; Orrit, M.; Talon, H. *Phys. Rev. Lett.* **1992** *69*, 1516.
(24) Basche, T.; Kummer, S.; Brauchle, C. *Nature* **1995**, *373*, 132.
(25) The equations in the bottom of Figure 1 are limited to $k_{exc} \ll k_{isc} + k_{rad} + k_{ic}$.
(26) Edman, L.; Mets, U.; Rigler, R. *Proc. Natl. Acad. Sci. U.S.A.* **1996**, *93*, 6710.
(27) Trautman, J. K. Spectroscopy and Dynamics of Single Molecules. Robert A. Welch Foundation Conference on Chemical Research Houston, TX, 1995.
(28) Marsella, M. J.; Fu, D. K.; Swager, T. M. *Adv. Mater.* **1995**, *7*, 145.
(29) Cook, R. J.; Kimble, H. J. *Phys. Rev. Lett.* **1985**, *54*, 1023.
(30) Equation 2d is limited to $k_{exc} \ll k_{isc} + k_{rad} + k_{ic}$.
(31) Nirmal, M.; Dabbousi, B. O.; Bawendi, M. G.; Macklin, J. J.; Trautman, J. K.; Harris, T. D.; Brus, L. E. *Nature* **1996**, *383*, 802.
(32) Maiti, S.; Haupts, U.; Webb, W. W. *Proc. Natl. Acad. Sci. U.S.A.* **1997**, *94*, 11753.
(33) Watanabe, A.; Kodaira, T.; Ito, O. *Chem. Phys. Lett.* **1997**, *273*, 227.
(34) Lanzani, G.; Nisoli, M.; Desilvestri, S.; Abbate, F. *Chem. Phys. Lett.* **1997**, *264*, 667.
(35) Blackford, J. W.; Jessen, S. W.; Lin, L. B.; Lih, J. J.; Gustafson, T. L.; Epstein, A. J.; Fu, D. K.; Marsella, M. J.; Swager, T. M.; Macdiarmid, A. G.; Yamaguchi, S.; Hamaguchi, H. *Phys. Rev. Lett.* **1996**, *76*, 1513.
(36) Rice, M. J.; Gartstein, Y. N. *Phys. Rev. B* **1996**, *53*, 10764.
(37) Esteghamatian, M.; Popovic, Z. D.; Xu, G. *J. Phys. Chem.* **1996**, *100*, 13716.
(38) Wagner, R. W.; Lindsey, J. S.; Seth, J.; Palaniappan, V.; Bocian, D. F. *J. Am. Chem. Soc.* **1996**, *118*, 3996.